



# Simulation of radiative heat transfer in microwave plasma chemical vapor deposition

Zhiguo Tian, Bin Liu, Moran Wang\*

Department of Engineering Mechanics, Tsinghua University, Beijing, 100084, China

## ARTICLE INFO

### Keywords:

Radiative heat transfer  
Diamond  
MPCVD  
3D simulation  
Infrared pyrometer

## ABSTRACT

Plasma, with temperature peaking around 3000 °C, plays a significant role in Microwave Plasma Chemical Vapor Deposition (MPCVD) for diamond production, while the radiative heat transfer process has not been extensively studied. In this work, we apply the Spherical Harmonics method, specifically the  $P_1$  approximation, to solve the Radiative Transfer Equation within the MPCVD simulation framework. This approach is integrated with the Maxwell's equations, the electron number density equation, the plasma temperature equation, and the solid temperature equation to obtain the temperature distribution of both plasma and diamond in a 3D cylindrical chamber. Our results show that the diamond temperature reaches a maximum at the center and decreases towards the edge, which aligns quantitatively with measurements from an infrared pyrometer. This accurate prediction of plasma and diamond temperature provides a powerful tool for optimizing MPCVD equipment and enhancing the production of large-size, high-quality diamonds or other products.

## 1. Introduction

Diamond is an excellent material for many engineering applications due to its extraordinary properties, such as quantum computing [1,2], detectors for high energy physics [3], biologically implantable electronics [4], semiconductor [5], thermal management [6,7] and so on. The Microwave Plasma Chemical Vapor Deposition (MPCVD) is the most promising method for producing man-made diamond [8–10]. However, large-size high-quality diamond is still unreachable and understanding the basic physical process in MPCVD is urging.

In MPCVD, the microwave, generally in 2.45 GHz, is imported into a resonant chamber and then concentrates in certain area, which can stimulate the gas mixture (typically  $H_2$  and  $CH_4$  at subatmospheric pressure) to generate plasma. Active carbon-containing groups in the plasma deposit on a substrate to produce diamond. In the whole process, plasma plays the key role since it, on the one hand, receives microwave energy and on the other hand provides carbon sources for the deposition. Previous experimental measurements demonstrate that the maximum plasma temperature can reach up to 3000 °C and the diamond temperature is typically around 1000 °C [9,11–14]. For such high temperature, the radiative heat transfer process becomes important. Besides, the surface reactions, whose rates depend on both the plasma and diamond temperature, directly determine the deposition rate [15,16]. Therefore, accurately predicting the plasma and diamond temperature simultaneously is significant for optimizing MPCVD.

Numerical simulation is a powerful tool because of MPCVD's complexity and high experimental cost. Fünér and his coworkers did pioneering work for MPCVD simulation, in which they assumed linear relationship between the electric field amplitude and the electron number density and successfully predicted the appearance of the possible secondary plasma for 2D axis-symmetric simulation in stationary condition [17,18]. Further, they introduced density gradient driven diffusion [19] and obtained more realistic result, which was followed by many researchers for its simplicity [20,21]. Modification has been made by cooperating the Arrhenius law and the Ohm's law into this model and can simulate spatial distribution of different active groups [22,23]. More detailed treatment of the chemical reactions was implemented mainly in 2D case because of the computation cost [24]. However, among all these simulations, they either ignored the plasma temperature distribution calculation or simply imposed a predefined diamond temperature value as the boundary condition [21,24–27]. Actually, the solid, especially the diamond, is heated by the plasma through thermal radiation and convection, and should be a posterior result, not a predefined condition.

For more realistic simulation, it is necessary to consider the radiative heat transfer process in spite of its complexity. Furthermore, experimental measurement of the diamond temperature should be provided for direct demonstration and comparison of the temperature spatial distribution. In this work, we implement infrared pyrometer measurement of the diamond temperature for MPCVD and simulate the

\* Corresponding author.

E-mail address: [mrwang@tsinghua.edu.cn](mailto:mrwang@tsinghua.edu.cn) (M. Wang).

temperature distribution, for the first time, by considering the radiative heat transfer process.

## 2. Method and equations

The most difficult part lies in the radiative heat transfer simulation, which needs to deal with the Radiative Transfer Equation (RTE) in participating media [28]. RTE is a complex differential-integral equation [28]:

$$\frac{dI_\eta}{ds} = \kappa_\eta I_{b\eta} - \beta_\eta I_\eta + \frac{\sigma_{s\eta}}{4\pi} \int_{4\pi} I_\eta(\vec{s}_i) \phi_\eta(\vec{s}_i, \vec{s}) d\Omega_i, \quad (1)$$

where  $I_\eta$  is the radiation intensity in wavenumber  $\eta$ ,  $I_{b\eta}$  is the blackbody's radiation intensity,  $\kappa_\eta$  is the absorption coefficient,  $\beta_\eta$  is the extinction coefficient,  $\sigma_{s\eta}$  is the scattering coefficient and  $d\Omega_i$  is the solid angle.  $\phi_\eta$  is the scattering phase function, which describes the probability of a ray from one direction,  $\vec{s}_i$ , being scattered into a certain other direction,  $\vec{s}$ . To solve the RTE, lots of numerical methods have been developed, including Spherical Harmonics method (P<sub>N</sub> approximation) [29], Discrete Ordinates method [30], Monte Carlo method [31], integral equation method [32], ray tracing-node analyzing method [33], Zonal method [28] and their combination [34,35]. Among them, the P<sub>1</sub> approximation, that is the simplest format of the Spherical Harmonics method, works well when the temperature field is known and is the easiest one to be implemented. In MPCVD, the plasma energy is transmitted by the microwave and its temperature can be obtained by properly modeling the microwave-plasma interaction. Therefore, the P<sub>1</sub> approximation is the most suitable one, as a first attempt, for cooperating the radiative heat transfer into MPCVD simulation.

In the Spherical Harmonics method, the radiation intensity is expanded by the two-dimensional generalized Fourier series [28]:

$$I(\vec{r}, \vec{s}) = \sum_{l=0}^{\infty} \sum_{m=-l}^l I_l^m(\vec{r}) Y_l^m(\vec{s}), \quad (2)$$

where  $I_l^m(\vec{r})$  is the position dependent coefficients,  $Y_l^m(\theta, \psi) = \begin{cases} \cos(l\psi) P_l^m(\cos\theta), & \text{for } m \geq 0 \\ \sin(l\psi) P_l^m(\cos\theta), & \text{for } m < 0 \end{cases}$ ,  $P_l^m(x) = (-1)^m \frac{(1-x^2)^{|m|/2}}{2^{|m|} l!} \frac{d^{l+|m|}}{dx^{l+|m|}} (x^2 - 1)^l$

is the associated Legendre polynomials. When the upper limit of  $l$  is 1,  $I(\vec{r}, \theta, \psi) = I_0^0 + I_1^0 \cos\theta + I_1^{-1} \sin\theta \sin\psi - I_1^1 \sin\theta \cos\psi$ , P<sub>1</sub> approximation is obtained by substituting this into Eq. (1) as [28]:

$$\frac{\partial}{\partial x_k} \left( -D_{P1} \frac{\partial G}{\partial x_k} \right) = -\kappa \left( G - 4\sigma T_g^4 \right), \quad (3)$$

where the Einstein summation rule is adopted and  $T_g$  is the plasma temperature,  $D_{P1} = \frac{1}{3\beta - A_1\sigma_s}$ ,  $\beta$ ,  $\sigma_s$ ,  $\kappa$  are the extinction coefficient, scattering coefficient and absorption coefficient integrated over wavenumber respectively,  $A_1$  is the linear-anisotropic scattering phase function coefficient, and  $\sigma$  is the Stefan-Boltzmann constant.  $G$  is the incident radiation, which is defined as  $G(\vec{r}) = \int_{4\pi} I(\vec{r}, \vec{s}) d\Omega$ . Eq. (3) is a single elliptic second-order partial differential equation in incident radiation, which is much easier to solve than Eq. (1), and therefore is the most commonly adopted form for studying radiation. Besides, it demonstrates acceptable precision compared with more complicated forms, like P<sub>3</sub> approximation or higher order formats, especially for the case when the temperature field is known [28].

By solving Eq. (3), the divergence of the radiation heat flux  $\vec{q}_r$  is obtained as [28]:

$$-\nabla \cdot \vec{q}_r = -\nabla \cdot (-D_{P1} \nabla G) = \kappa \left( G - 4\sigma T_g^4 \right), \quad (4)$$

which behaves as a heat sink for plasma temperature equation. The other heat source for plasma temperature is from the microwave-plasma interaction. Regarding the plasma as a dielectric material [36], the heat source term can be obtained by the Ohm's law as  $\frac{1}{2} \frac{e^2 n_e v_e}{m_e (v_e^2 + \omega^2)}$

$|E|^2$ , where  $n_e$  is the electron number density,  $v_e$  is the effective collision frequency of the electrons with other particles,  $\omega$  is the microwave frequency,  $|E|$  is the electric field amplitude,  $e$  is the electron's charge and  $m_e$  is the electron's mass [37]. Therefore, the plasma temperature equation is:

$$\frac{\partial}{\partial x_k} \left( -\lambda_g \frac{\partial T_g}{\partial x_k} \right) = \frac{1}{2} \frac{e^2 n_e v_e}{m_e (v_e^2 + \omega^2)} |E|^2 + \kappa \left( G - 4\sigma T_g^4 \right), \quad (5)$$

where  $\lambda_g$  is the thermal conductivity of the plasma which is typically calculated by theoretically solving the electron Boltzmann equation [38].

The electric field amplitude is obtained by solving the Maxwell's equation in frequency domain [39]:

$$\nabla \times \left( \mu_{em}^{-1} (\nabla \times \vec{E}) \right) + \left( j\omega \frac{e^2 n_e}{m_e (v_e + j\omega)} - \omega^2 \epsilon_{em} \right) \vec{E} = 0, \quad (6)$$

where  $\mu_{em}$  is the relative magnetic permeability of plasma,  $\epsilon_{em}$  is the relative electric permittivity of plasma and  $j$  is the imagination unit.  $\mu_{em}$  and  $\epsilon_{em}$  are assumed to be 1 for the gas in our present work.  $\vec{E}$  is the time-independent electric field magnitude. Here, the plasma is equivalent to a dielectric, whose electric conductivity is related to the electron number density and is expressed as  $\sigma_{em,p} = \frac{e^2 n_e v_e}{m_e (v_e^2 + \omega^2)}$  [37].

The electron number density equation for plasma is obtained by a simplified macroscopical model, sparing the effort of simulating the complex chemical reactions [18,19,21]:

$$\frac{\partial}{\partial x_k} \left( -D_e \frac{\partial n_e}{\partial x_k} \right) = R_i |E|^2 n_e - R_{vr} n_e^2, \quad (7)$$

where  $D_e$  is the diffusion coefficient of electron,  $R_i$  is the ionization rate and  $R_{vr}$  is the recombination rate. This is a simplified model for microwave plasma simulation. The left side of Eq. (7) is the diffusion process driven by the density gradient and the right side of Eq. (7) means the source term of electron, which is a balance between production and loss of electron. Microscopically, the plasma is generated from electron collisions, in which the free electrons in the gas mixture obtain energy from the microwave and high-speed velocity electrons collide with the gas molecules to generate more electrons and ions. The production of electron is such process that an electron collides with a neutral molecule or a charged ion to produce a secondary electron. It is subsequently proportional to electron number density and electron energy, where electron energy is gained from the electric field and should be proportional to electric magnitude squared, which is quantified as  $R_i |E|^2 n_e$ . On the other hand, an electron collides with a charged ion and forms a new neutral molecule or a new charged ion, which is called as the recombination process and causes the loss of electron. The recombination process is quantitatively expressed as  $R_{vr} n_e^2$ . The balance of production and loss leads to the final state of plasma [40].

The solid temperature equation is the heat equation without any heat source:

$$\frac{\partial}{\partial x_k} \left( -\lambda_s \frac{\partial T_s}{\partial x_k} \right) = 0, \quad (8)$$

where  $\lambda_s$  is the thermal conductivity of the solid and  $T_s$  is the solid temperature.

The boundary conditions for the above equations are listed as follows.

Ideal conductor wall for Eq. (6):

$$\vec{n}_b \times \vec{E} = 0, \quad (9)$$

where  $\vec{n}_b$  is the normal vector for the wall. The microwave excitation is imported from a microwave source and is realized by the S-parameters calculation numerically [39].

Dirichlet boundary condition for the electron number density, Eq. (7), is:

$$n_{eb} = 0. \quad (10)$$

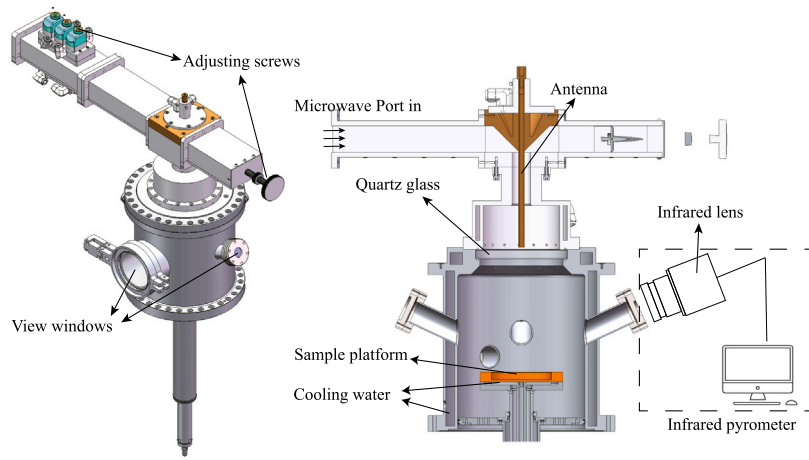


Fig. 1. MPCVD apparatus and infrared pyrometer measurement.

This boundary condition is chosen because the MPCVD equipment is linked with the ground and all the electrons are directed away to the ground very quickly.

Third kind boundary condition for the radiation  $P_1$  approximation, Eq. (3), is [28]:

$$-\vec{n}_b \cdot \left( -D_{P1} \frac{\partial G}{\partial x_k} \right) = 4\sigma T_{sb}^4 - G, \quad (11)$$

where  $T_{sb}$  is the wall temperature of the plasma region. The original form of Eq. (11) is  $-\frac{2-\epsilon}{\epsilon} \vec{n}_b \cdot \left( -D_{P1} \frac{\partial G}{\partial x_k} \right) = 4\sigma T_{sb}^4 - G$ , where  $\epsilon$  is the wall emittance. We set  $\epsilon$  to be 1, because: the emittance of diamond increases with temperature [41], in which the emittance is close to 1 when the wavelength is 5  $\mu\text{m}$  and temperature is 350  $^\circ\text{C}$ . Therefore, the emittance  $\epsilon$  is safe to be assumed as 1 since the diamond temperature is larger than 700  $^\circ\text{C}$  in MPCVD and the wavelength range of our Infrared Pyrometer is 4.8–5.2  $\mu\text{m}$ .

Based on the boundary condition (11), radiation and convection heat flux for the plasma temperature Eq. (5) is obtained as:

$$-\vec{n}_b \cdot \left( -\lambda_g \frac{\partial T_g}{\partial x_k} \right) = \kappa (G - 4\sigma T_{sb}^4) - h (T_g - T_{g,ref}), \quad (12)$$

where  $h$  is the convective heat transfer coefficient, and  $T_{g,ref}$  is the reference temperature which is assigned as 1000 K. Similarly, the boundary condition for the solid temperature Eq. (8) is:

$$-\vec{n}_b \cdot \left( -\lambda_s \frac{\partial T_s}{\partial x_k} \right) = \kappa (G - 4\sigma T_{sb}^4) - h (T_s - T_{g,ref}). \quad (13)$$

This boundary condition, Eq. (13), provides heat source for the solid parts, especially heating the diamonds, which demonstrates the heating effect by thermal radiation and convection.

The above equations are closed and we can solve them numerically.

### 3. Experimental and numerical set-up

Fig. 1 demonstrates the MPCVD apparatus and infrared pyrometer for our present study. For the MPCVD, the microwave, with frequency of 2.45 GHz and maximum power of 10 kW, is imported into a cylindrical chamber through a BJT26 waveguide and an antenna. The adjusting screws are used for controlling the reflecting microwave power in actual production. The whole chamber is separated by a quartz glass and the downside of the chamber is full of gas mixture, whose components are  $\text{H}_2$  and  $\text{CH}_4$ , possibly with small addition of  $\text{N}_2$ ,  $\text{O}_2$ ,  $\text{Ar}$ . The gas pressure is kept at 22 kPa as the growing condition. The seed diamonds, generally in square form with 7 mm length, are put onto the sample platform. The working principle of the Infrared Pyrometer (IR) is that the thermal radiation is collected by the IR camera and it is correlated to the target surface temperature by the Planck's law. We choose the working wavelength of the IR camera to be 4.8–5.2  $\mu\text{m}$ . That

is because: the emittance of diamond increases with temperature [41], in which the emittance is close to 1 when the wavelength is 5  $\mu\text{m}$  and temperature is 350  $^\circ\text{C}$ . Additionally, the plasma in MPCVD typically emits radiation with wavelength smaller than 1  $\mu\text{m}$ . Therefore, we choose the IR camera with working wavelength 4.8–5.2  $\mu\text{m}$ . Then, the emittance is safe to be assumed as 1 since the diamond temperature is larger than 700  $^\circ\text{C}$  in MPCVD, which is also self-consistent with our numerical simulation as boundary condition (11). Meanwhile, the plasma interference is very small for wavelength range of 4.8–5.2  $\mu\text{m}$ . The IR camera is calibrated standardly by measuring a known black-body temperature and its measurement range is 400–1100  $^\circ\text{C}$ . The IR camera is placed near the view window for non-contact temperature measurement of the diamonds and collects the infrared signal from the chamber. The measured temperature distribution is displayed on the computer screen.

From the actual apparatus, we can extract the inner structure for numerical simulation, as Fig. 2 shows. The MPCVD chamber is separated by a quartz glass and only the downside part contains the gas, which is noted as the plasma region in Fig. 2. The largest radius in the plasma region is 11 cm. The electric field, Eq. (6), is solved in the whole domain, named as the electric region, and the microwave is ported in as an excitation source, which is realized by the S-parameters calculation numerically. In the plasma region, the electron number density Eq. (7), the  $P_1$  approximation Eq. (3) and the plasma temperature Eq. (5) are solved. The solid temperature Eq. (8) is imposed on the platform and the diamonds, noted as the solid region in Fig. 2. The corresponding boundary conditions for the equations are demonstrated by different dash lines. The inside of the stainless steel platform is the cooling water. For simplicity, we do not simulate the water flow, but only impose convective heat transfer boundary condition in this part. 34 diamonds are placed on a molybdenum platform which precisely consists with actual production process. By the way, this actual placement of diamonds is the reason for conducting three-dimensional simulations.

### 4. Results and discussion

#### 4.1. Infrared pyrometer result

The temperature profile obtained from the infrared pyrometer is demonstrated in Fig. 3. The photo clearly displays the temperature distribution of the diamonds is not uniform, with largest value of 1033.1  $^\circ\text{C}$  in center, as Fig. 3(a). The average temperature values for each diamond are recorded and then plotted in 3D surface contour as Fig. 3 (b). This measurement result strongly demonstrates that the diamond temperatures are not equal. In previous simulation, the diamond temperatures are assumed to be a constant value and a Dirichlet

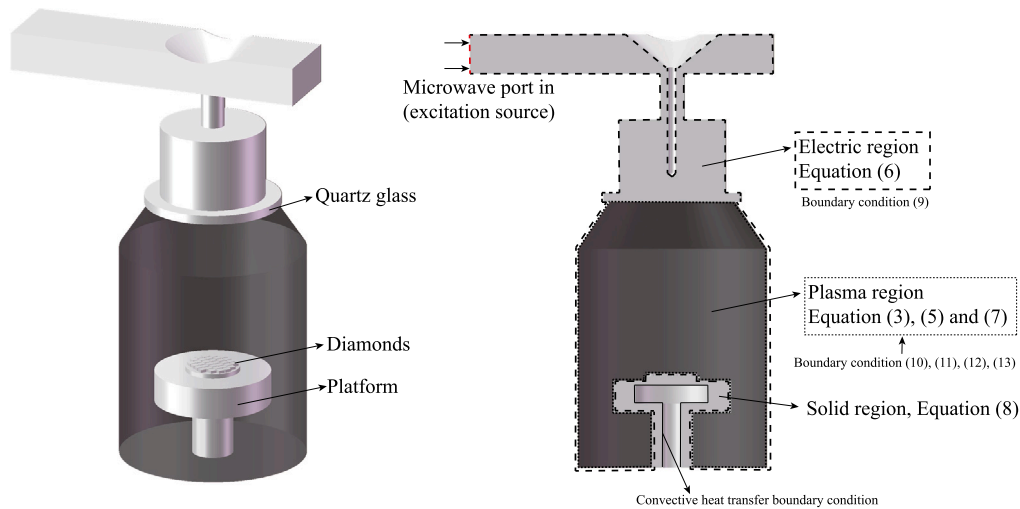


Fig. 2. Inner structure of the MPCVD for numerical simulation.

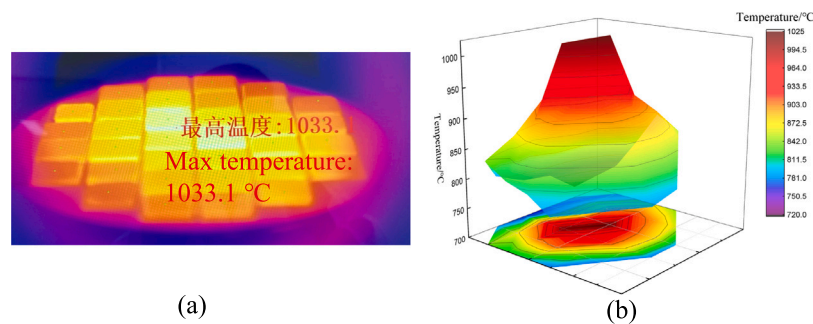


Fig. 3. Infrared pyrometer measurement result: (a) Photo by the IR camera; (b) 3D surface plot of the measured temperature.

boundary condition is imposed [21,24,25,27], which can simplify the simulation but is non-physical. Actually, the diamond temperatures are affected by the plasma's temperature, through radiation and convection heat transfer, and should be a posterior result, not a predetermined condition. Besides, the diamond temperature directly influences the deposition rate [15,16] and determines the quality of diamonds. This non-uniform distribution should be avoided in actual production and accurate prediction of this temperature distribution is important for equipment design and optimization.

#### 4.2. Simulation result

In our simulation, the diamond temperatures are not predefined. Rather, we impose radiation and convection heat transfer boundary condition for diamond surfaces, as Eq. (13). The parameter values for our numerical simulation are listed in Table 1. The MPCVD plasma is an optically thin medium and it is weakly scattering. We adopt Finite Element Method (FEM) by COMSOL 6.1 to numerically solve the equation set.

First, the mesh independence test is presented as Fig. 4. Seven different unstructured meshes are generated with mesh number as 99 502, 162 228, 279 698, 402 428, 498 992, 768 635, 921 186. For quantitative comparison, a 3D point, which is 20 mm above the center of the platform, is monitored. Different variables, including the plasma temperature  $T_g$ , electric field amplitude  $|E|$ , electron number density  $n_e$ , and incident radiation  $G$  are recorded. For unified display of results, dimensionless variables, which are calculated by dividing the value with the one of the finest mesh case 921 186, are adopted. Fig. 4 illustrates that the differences decrease with the increase of the mesh

number and dimensionless variables values converge to 1 with small oscillation. Based on Fig. 4, we choose the mesh number to be 921 186 and the results presented in Fig. 5 all adopt this mesh number.

Our simulation results are plotted in Fig. 5. The electric field amplitude, in Fig. 5(a), demonstrates that the microwave is imported through a waveguide and enters a resonant chamber, where the microwave concentrates above the sample platform. This area of concentrated electric field stimulates the generation of the plasma, as Fig. 5(b) shows. Previous experimental results, which are obtained by Optical Emission Spectroscopy (OES) [42], millimeter-wave open resonator [43], and Thomson scattering measurement [44], consistently demonstrate that the maximum of the electron number density for typical MPCVD is on the magnitude of  $10^{17} \text{ m}^{-3}$ . In our simulation, Fig. 5(b), the maximum of the electron number density is also  $10^{17} \text{ m}^{-3}$  and it consists with the previous experiments. These electrons are accelerated by the microwave and can heats the plasma through the Ohm's law, by considering the plasma as a dielectric medium [36,37]. On the other hand, when the plasma temperature is high, the radiation becomes increasingly important. Therefore, we incorporate the radiation into our simulation, as Eqs. (3) and (5), and the corresponding simulation results are demonstrated as Fig. 5(c), (d), (e), (f) and (g). The maximum plasma temperature is about 3700 K which is also consistent with previous experimental measurements [9,11–14]. The electrical conductivity is calculated as  $\sigma_{\text{em,p}} = \frac{e^2 n_e v_e}{m_e (v_e^2 + u^2)}$  [37] and it exhibits similar distribution

as the electron number density. The heat sink caused by radiation, Eq. (4), is plotted as Fig. 5 (f), which is negative. Besides, this heat sink is comparable with the total heat source in Eq. (5), expressed as

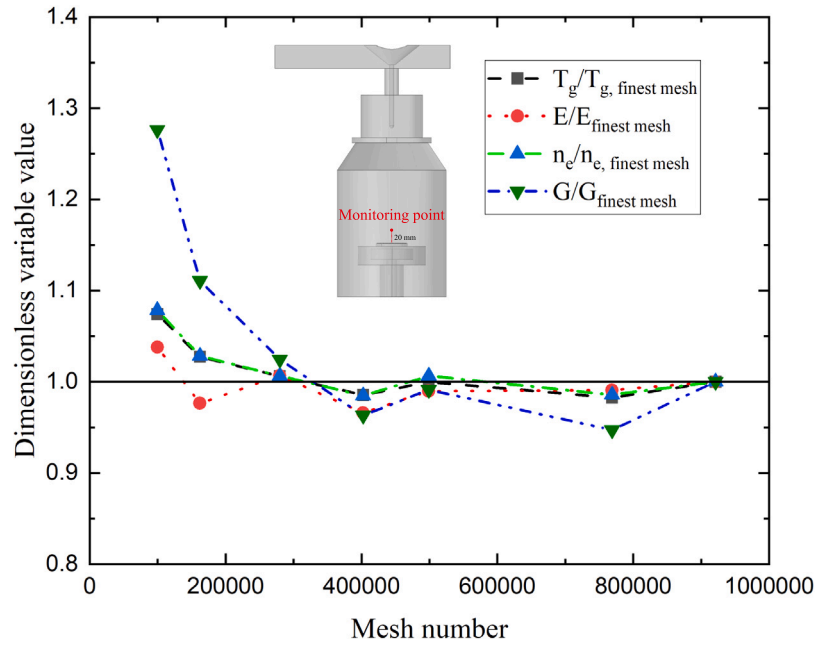


**Fig. 4.** Mesh independence test results. 7 different meshes are generated with mesh number as 99 502, 162 228, 279 698, 402 428, 498 992, 768 635, 921 186. A 3D point, which is 20 mm above the center of the platform, is monitored. Different variables, including the plasma temperature  $T_g$ , electric field amplitude  $|E|$ , electron number density  $n_e$ , and incident radiation  $G$  are recorded and presented by dimensionless variables, which are calculated by dividing the value with the one of the finest mesh, 921 186.

**Table 1**  
Parameter values in numerical simulation.

Parameter	Value	Comments
$D_e$	$0.2 \text{ m}^2 \text{ s}^{-1}$	Theoretically estimated value for plasma temperature of 4000 K [38,45]
$R_{er}$	$1 \times 10^{-13} \text{ m}^{-3} \text{ s}^{-1}$	Extrapolation of experimental data [46]
$R_i$	$3 \times 10^{-6} \text{ m}^{-3} \text{ s}^{-1}$	Estimation from experimental measurement of electron number density [42]
$P_{in}$	9000 W	Microwave power in our own experiment
$v_e$	$1 \times 10^{11} \text{ s}^{-1}$	Theoretical calculated value when electron energy is 1 eV and gas density is $10^{24} \text{ m}^{-3}$ [24]
$\lambda_{\text{diamond}}$	$200 \text{ W m}^{-1} \text{ K}^{-1}$	Interpolation of experimental data when temperature is 1300 K [47]
$\lambda_{\text{plasma}}$	$1.5 \text{ W m}^{-1} \text{ K}^{-1}$	Theoretically estimated value for plasma temperature of 4000 K [38]
$\kappa$	$0.4 \text{ m}^{-1}$	Typical estimated absorption coefficient for MPCVD plasma [28,48]
$h_{\text{plasma}}$	$10 \text{ W m}^{-2} \text{ K}^{-1}$	Theoretically estimated value for plasma temperature of 4000 K [38]
$h_{\text{water}}$	$150 \text{ W m}^{-2} \text{ K}^{-1}$	Estimation for our experimental condition which is forced convection but close to natural convection [49]
$D_{pl}$	0.01 m	Calibrated value [28]

$\frac{1}{2} \frac{e^2 n_e v_e}{m_e (v_e^2 + u^2)} |E|^2 + \kappa (G - 4\sigma T_g^4)$ , which demonstrates the necessity for considering radiative heat transfer in MPCVD simulation.

The diamonds temperature is finally obtained as Fig. 5(h). In our simulation, we do not predefine the diamonds temperature, and the diamonds are heated by the plasma through radiation and convection, as the boundary condition Eq. (13) demonstrates. Our simulation results show that the diamonds temperature has largest value in the central area and gradually decreases towards the edge. The maximum simulation temperature is about 1000 °C, which quantitatively agrees with the infrared pyrometer measurement result in Fig. 3. Due to this non-uniform temperature distribution, the thermal management of the MPCVD is important in actual manufacture and accurate prediction of the temperature is extremely important for equipment design and optimization. Our simulation framework provides a useful tool for designing MPCVD apparatus.

Relative error  $\frac{T_{\text{exp}} - T_{\text{sim}}}{T_{\text{exp}}} \times 100\%$  between the infrared pyrometer measurement ( $T_{\text{exp}}$ ) and numerical simulation ( $T_{\text{sim}}$ ) in 3D surface plot

is demonstrated in Fig. 5(i). For every single diamond, the measured and simulated temperature are averaged and then plotted. The result illustrates that the maximum relative temperature difference is about -10%, which is generally acceptable for plasma simulation. Besides, we adopt the  $P_1$  approximation with effective parameters of plasma in our simulation and higher order format, like  $P_3$  approximation, or more careful consideration of the radiation parameters might decrease the relative temperature difference. Furthermore, the plasma environment affects the infrared pyrometer measurement and raises measurement uncertainty, which also accounts for the Relative error. Still, the comparison validates our simulation, whose maximum deviation from infrared pyrometer measurement is within 10%.

## 5. Conclusion

Our present work incorporates radiative heat transfer process in MPCVD simulation, for the first time, with a simple  $P_1$  approximation

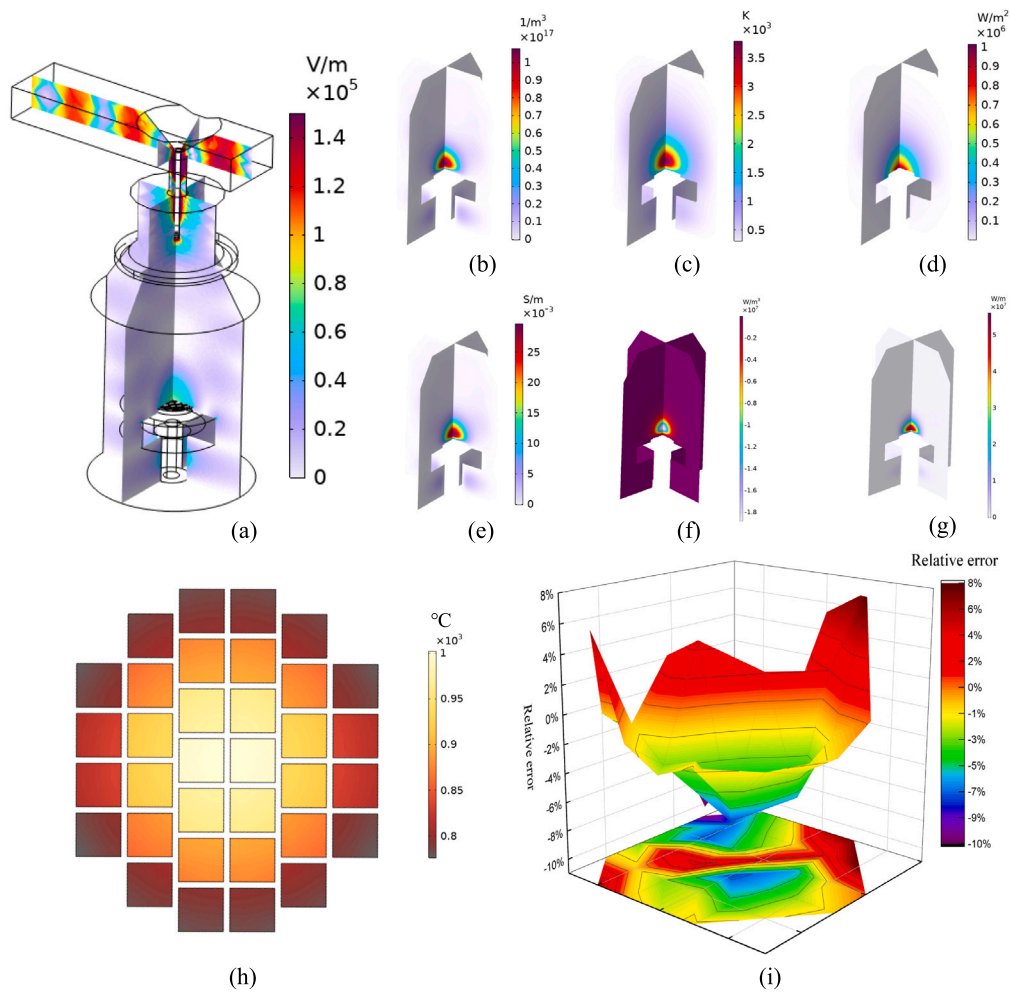


**Fig. 5.** Simulation results and comparison with experiment: (a) Electric field amplitude  $|E|$ ; (b) Electron number density  $n_e$ ; (c) Plasma temperature  $T_g$ ; (d) Incident radiation  $G$ ; (e) Electrical conductivity  $\sigma_{em,p}$ ; (f) Heat sink by radiation  $\nabla \cdot \vec{q}_r$ , Eq. (4); (g) Total heat source in Eq. (5), expressed as  $\frac{1}{2} \frac{e^2 n_e v_e}{m_e (v_e^2 + u^2)} |E|^2 + \kappa (G - 4\sigma T_g^4)$ ; (h) Diamonds temperature  $T_{sim}$ , which is  $T_s$  for the upper surface of all diamonds; (i) Relative error  $\frac{T_{exp} - T_{sim}}{T_{exp}} \times 100\%$  between the infrared pyrometer measurement  $T_{exp}$  and our numerical simulation  $T_{sim}$ .

of the Radiative Transfer Equation. By solving the Maxwell's equations, the electron number density equation, the plasma temperature equation, the  $P_1$  approximation, and the solid temperature equation with proper boundary conditions, we accurately predict the plasma and diamond temperature simultaneously. Additionally, infrared pyrometer measurements conducted during the actual production process visually confirm the non-uniform distribution of diamond temperature, strongly supporting our simulation results. This finding provides a powerful tool for the design and optimization of MPCVD equipment and production process.

#### CRediT authorship contribution statement

**Zhiguo Tian:** Writing – original draft, Software, Investigation. **Bin Liu:** Writing – review & editing, Validation. **Moran Wang:** Writing – review & editing, Supervision, Project administration, Conceptualization.

#### Declaration of competing interest

The authors declare that they have no known competing financial interests or personal relationships that could have appeared to influence the work reported in this paper.

#### Funding

This work is financially supported by the NSF of China (No. 1243 2013, 12272207) and the Tsinghua University Initiative Scientific Research Program for financial support.

#### Data availability

No data was used for the research described in the article.

#### References

- [1] L. Childress, R. Hanson, Diamond NV centers for quantum computing and quantum networks, *MRS Bull.* 38 (2) (2013) 134–138.
- [2] T. Schröder, M.E. Trusheim, M. Walsh, L. Li, J. Zheng, M. Schukraft, A. Sipahigil, R.E. Evans, D.D. Sukachev, C.T. Nguyen, et al., Scalable focused ion beam creation of nearly lifetime-limited single quantum emitters in diamond nanostructures, *Nat. Commun.* 8 (1) (2017) 15376.
- [3] N. Skukan, V. Grilj, I. Sudić, M. Pomorski, W. Kada, T. Makino, Y. Kambayashi, Y. Andoh, S. Onoda, S. Sato, et al., Charge multiplication effect in thin diamond films, *Appl. Phys. Lett.* 109 (4) (2016) 043502.
- [4] A. Ahnood, M. Escudie, R. Cicione, C. Abeyratne, K. Ganesan, K. Fox, D. Garrett, A. Stacey, N. Apollo, S. Lichter, et al., Ultrananocrystalline diamond-CMOS device integration route for high acuity retinal prostheses, *Biomed. Microdevices* 17 (2015) 1–11.

- [5] M.W. Geis, T.C. Wade, C.H. Wuorio, T.H. Fedynshyn, B. Duncan, M.E. Plaut, J.O. Varghese, S.M. Warnock, S.A. Vitale, M.A. Hollis, Progress toward diamond power field-effect transistors, *Phys. Status Solidi A* 215 (22) (2018) 1800681.
- [6] B. Wang, X. Xu, Y. He, N. Rodionov, J. Zhu, Synergistic competition mechanism of phonon scattering in uniaxial (100) strain diamond: A first-principles study, *Int. J. Heat Mass Transfer* 216 (2023) 124598.
- [7] B. Liu, M. Wang, Interfacial thermal transport driven by phonon wave behaviors and its tunability in GaN-on-diamond devices, *Int. J. Heat Mass Transfer* 229 (2024) 125700.
- [8] M. Kamo, H. Yurimoto, Y. Sato, Epitaxial growth of diamond on diamond substrate by plasma assisted CVD, *Appl. Surf. Sci.* 33 (1988) 553–560.
- [9] A. Bolshakov, V. Ralchenko, G. Shu, B. Dai, V.Y. Yurov, E. Bushuev, A. Khomich, A. Altakhov, E. Ashkinazi, I. Antonova, et al., Single crystal diamond growth by MPCVD at subatmospheric pressures, *Mater. Today Commun.* 25 (2020) 101635.
- [10] S.V. Baryshev, M. Muehle, Scalable production and supply chain of diamond wafers using microwave plasma: A mini-review, *IEEE Trans. Plasma Sci.* 52 (2023) 1082–1103.
- [11] D.S. Green, T.G. Owano, S. Williams, D.G. Goodwin, R.N. Zare, C.H. Kruger, Boundary layer profiles in plasma chemical vapor deposition, *Science* 259 (5102) (1993) 1726–1729.
- [12] A. Gicquel, K. Hassouni, S. Farhat, Y. Breton, C. Scott, M. Lefebvre, M. Pealat, Spectroscopic analysis and chemical kinetics modeling of a diamond deposition plasma reactor, *Diam. Relat. Mater.* 3 (4–6) (1994) 581–586.
- [13] A. Gicquel, M. Chenevier, Y. Breton, M. Petiau, J. Booth, K. Hassouni, Ground state and excited state H-atom temperatures in a microwave plasma diamond deposition reactor, *J. Phys. III* 6 (9) (1996) 1167–1180.
- [14] J. Ma, M.N. Ashfold, Y.A. Mankelevich, Validating optical emission spectroscopy as a diagnostic of microwave activated CH<sub>4</sub>/Ar/H<sub>2</sub> plasmas used for diamond chemical vapor deposition, *J. Appl. Phys.* 105 (4) (2009) 043302.
- [15] D. Goodwin, Scaling laws for diamond chemical-vapor deposition. II. Atomic hydrogen transport, *J. Appl. Phys.* 74 (11) (1993) 6895–6906.
- [16] D.G. Goodwin, Scaling laws for diamond chemical-vapor deposition. I. Diamond surface chemistry, *J. Appl. Phys.* 74 (11) (1993) 6888–6894.
- [17] M. Fünler, C. Wild, P. Koidl, Numerical simulations of microwave plasma reactors for diamond CVD, *Surf. Coat. Technol.* 74 (1995) 221–226.
- [18] M. Fünler, C. Wild, P. Koidl, Simulation and development of optimized microwave plasma reactors for diamond deposition, *Surf. Coat. Technol.* 116 (1999) 853–862.
- [19] E. Pleuler, C. Wild, M. Fünler, P. Koidl, The CAP-reactor, a novel microwave CVD system for diamond deposition, *Diam. Relat. Mater.* 11 (3–6) (2002) 467–471.
- [20] X. Li, W. Tang, F. Wang, C. Li, L. Hei, F. Lu, A compact ellipsoidal cavity type microwave plasma reactor for diamond film deposition, *Diam. Relat. Mater.* 20 (3) (2011) 374–379.
- [21] Z. Zhai, C. Zhang, B. Chen, Y. Xiong, Y. Liang, L. Liu, B. Yang, N. Yang, X. Jiang, N. Huang, Covalently-bonded diaphite nanoplatelet with engineered electronic properties of diamond, *Adv. Funct. Mater.* (2024) 2401949.
- [22] H. Yamada, A. Chayahara, Y. Mokuno, Simplified description of microwave plasma discharge for chemical vapor deposition of diamond, *J. Appl. Phys.* 101 (6) (2007) 063302.
- [23] H. Yamada, A. Chayahara, Y. Mokuno, S. Shikata, Numerical microwave plasma discharge study for the growth of large single-crystal diamond, *Diam. Relat. Mater.* 54 (2015) 9–14.
- [24] K. Hassouni, F. Silva, A. Gicquel, Modelling of diamond deposition microwave cavity generated plasmas, *J. Phys. D: Appl. Phys.* 43 (15) (2010) 153001.
- [25] K. Hassouni, T. Grotjohn, A. Gicquel, Self-consistent microwave field and plasma discharge simulations for a moderate pressure hydrogen discharge reactor, *J. Appl. Phys.* 86 (1) (1999) 134–151.
- [26] H. Yamada, A. Chayahara, Y. Mokuno, Y. Soda, Y. Horino, N. Fujimori, Numerical analysis of power absorption and gas pressure dependence of microwave plasma using a tractable plasma description, *Diam. Relat. Mater.* 15 (9) (2006) 1395–1399.
- [27] J. Su, Y. Li, X. Li, P. Yao, Y. Liu, M. Ding, W. Tang, A novel microwave plasma reactor with a unique structure for chemical vapor deposition of diamond films, *Diam. Relat. Mater.* 42 (2014) 28–32.
- [28] M.F. Modest, S. Mazumder, *Radiative Heat Transfer*, Elsevier, New York, 2021.
- [29] Y. Sun, S. Zheng, B. Jiang, J. Tang, F. Liu, One-dimensional P1 method for gas radiation heat transfer in spherical geometry, *Int. J. Heat Mass Transfer* 145 (2019) 118777.
- [30] R.-R. Zhou, B.-W. Li, The modified discrete ordinates method for radiative heat transfer in two-dimensional cylindrical medium, *Int. J. Heat Mass Transfer* 139 (2019) 1018–1030.
- [31] B. Liu, J. Zhao, S. Grigoriev, A. Gusarov, Particle non-isothermality effect on the radiative thermal conductivity in dense particulate systems, *Int. J. Heat Mass Transfer* 204 (2023) 123822.
- [32] B.-H. Gao, H. Qi, Y. Zhao, Y.-T. Ren, M.-J. He, An efficient equation-solving method for calculating radiative transfer in isotropic scattering medium, *Int. J. Heat Mass Transfer* 174 (2021) 121298.
- [33] J.-F. Luo, S.-L. Chang, J.-K. Yang, J.-C. Yang, Conduction and radiation in a rectangular isotropic scattering medium with black surfaces by the RTNAM, *Int. J. Heat Mass Transfer* 52 (21–22) (2009) 5064–5071.
- [34] M. Luo, C. Wang, J. Zhao, L. Liu, Characteristics of effective thermal conductivity of porous materials considering thermal radiation: A pore-level analysis, *Int. J. Heat Mass Transfer* 188 (2022) 122597.
- [35] Z.-C. Jin, F.-X. Sun, X.-L. Xia, C. Sun, Numerical investigation of evaporation and radiation absorption of a non-spherical water droplet under asymmetrically radiative heating, *Int. J. Heat Mass Transfer* 140 (2019) 66–79.
- [36] F.F. Chen, et al., *Introduction to Plasma Physics and Controlled Fusion*, vol. 1, Springer, Switzerland, 1984.
- [37] G. Hagelaar, K. Hassouni, A. Gicquel, Interaction between the electromagnetic fields and the plasma in a microwave plasma reactor, *J. Appl. Phys.* 96 (4) (2004) 1819–1828.
- [38] M.I. Boulos, P.L. Fauchais, E. Pfender, Transport properties of gases under plasma conditions, in: *Handbook of Thermal Plasmas*, Springer, Switzerland, 2023, pp. 257–309.
- [39] D.B. Davidson, *Computational Electromagnetics for RF and Microwave Engineering*, Cambridge University Press, New York, 2010.
- [40] M.A. Lieberman, A.J. Lichtenberg, *Principles of Plasma Discharges and Materials Processing*, John Wiley Sons, Inc., New Jersey, 2005.
- [41] T. Mollart, K. Lewis, The infrared optical properties of CVD diamond at elevated temperatures, *Phys. Status Solidi A* 186 (2) (2001) 309–318.
- [42] N. Derkaoui, C. Rond, T. Gries, G. Henrion, A. Gicquel, Determining electron temperature and electron density in moderate pressure H<sub>2</sub>/CH<sub>4</sub> microwave plasma, *J. Phys. D: Appl. Phys.* 47 (20) (2014) 205201.
- [43] T. Grotjohn, J. Asmussen, J. Sivagnaname, D. Story, A. Vikharev, A. Gorbachev, A. Kolysko, Electron density in moderate pressure diamond deposition discharges, *Diam. Relat. Mater.* 9 (3–6) (2000) 322–327.
- [44] S. Narishige, S. Suzuki, M.D. Bowden, K. Uchino, K. Muraoka, T. Sakoda, W.Z. Park, Thomson scattering measurement of electron density and temperature of a microwave plasma produced in a hydrogen gas at a moderate pressure, Japan. *J. Appl. Phys.* 39 (12R) (2000) 6732.
- [45] G. Hagelaar, L.C. Pitchford, Solving the Boltzmann equation to obtain electron transport coefficients and rate coefficients for fluid models, *Plasma Sources Sci. Technol.* 14 (4) (2005) 722.
- [46] J. Glosik, O. Novotný, A. Pysanenko, P. Zakouril, R. Plašil, P. Kudrna, V. Poterya, The recombination of and ions with electrons in hydrogen plasma: dependence on temperature and on pressure of H<sub>2</sub>, *Plasma Sources Sci. Technol.* 12 (4) (2003) S117.
- [47] L. Wei, P. Kuo, R. Thomas, T. Anthony, W. Banholzer, Thermal conductivity of isotopically modified single crystal diamond, *Phys. Rev. Lett.* 70 (24) (1993) 3764.
- [48] R. Soloukhin, Y.A. Yacobi, Hydrogen plasma absorption coefficients at laser frequencies, *J. Quant. Spectrosc. Radiat. Transfer* 12 (1) (1972) 25–34.
- [49] E. EDGE, Overall heat transfer coefficients table and equation, 2024, <https://www.engineersedge.com/thermodynamics/overall-heat-transfer-table.htm>.